

RESEARCH ARTICLE

10.1002/2016JD025863

Key Points:

- Higher-frequency luminosity components (300 kHz) propagate with faster phase velocity (80% faster) than lower frequency components (50 kHz)
- On average, frequency domain group velocities exceed phase velocities by approximately 44%
- Averaged over all heights, higher-frequency luminosity components attenuate approximately 3 times faster than lower frequency components

Correspondence to:

F. L. Carvalho,
fcarval1@ufl.edu

Citation:

Carvalho, F. L., M. A. Uman, D. M. Jordan, and R. C. Moore (2017), Frequency domain analysis of triggered lightning return stroke luminosity velocity, *J. Geophys. Res. Atmos.*, 122, 2334–2350, doi:10.1002/2016JD025863.

Received 29 AUG 2016

Accepted 30 JAN 2017

Accepted article online 1 FEB 2017

Published online 16 FEB 2017

Frequency domain analysis of triggered lightning return stroke luminosity velocity

F. L. Carvalho¹ , M. A. Uman¹ , D. M. Jordan¹ , and R. C. Moore¹ 

¹Department of Electrical and Computer Engineering, University of Florida, Gainesville, Florida, USA

Abstract Fourier analysis is applied to time domain return stroke luminosity signals to calculate the phase and group velocities and the amplitude of the luminosity signals as a function of frequency measured between 4 m and 115 m during 12 triggered lightning strokes. We show that pairs of time domain luminosity signals measured at different heights can be interpreted as the input and the output of a system whose frequency domain transfer function can be determined from the measured time domain signals. From the frequency domain transfer function phase we find the phase and group velocities, and luminosity amplitude as a function of triggered lightning channel height and signal frequency ranging from 50 kHz to 300 kHz. We show that higher-frequency luminosity components propagate faster than the lower frequency components and that higher-frequency luminosity components attenuate more rapidly than lower frequency components. Finally, we calculate time domain return stroke velocities as a function of channel height using two time delay techniques: (1) measurement at the 20% amplitude level and (2) cross correlation.

1. Introduction

The propagation speed of lightning return strokes has been measured by using both streak photography [e.g., *Schonland*, 1956; *Boyle and Orville*, 1976; *Hubert and Mouget*, 1981; *Idone and Orville*, 1982; *Idone et al.*, 1984; *Willett et al.*, 1988] and photoelectric techniques [e.g., *Mach and Rust*, 1989; *Olsen et al.*, 2004; *Wang et al.*, 2013; *Carvalho et al.*, 2014, 2015]. The speed has been measured either between the first luminous signal above threshold at different heights [e.g., *Schonland*, 1956], at some percentage of the peak luminosity [e.g., *Carvalho et al.*, 2015], or by extrapolating the primary slope of the luminosity rise-to-peak to the zero-luminosity level [e.g., *Olsen et al.*, 2004; *Wang et al.*, 2004]. The upward speed of the return stroke luminosity has usually been assumed to be the speed of the electrical current, a parameter needed for lightning return stroke modeling [e.g., *Willett et al.*, 1988; *Krider*, 1992, 1994; *Thottappillil and Uman*, 1993; *Chen and Zhu*, 2014], although this equivalence has recently been shown not to be the case [e.g., *Liang et al.*, 2014; *Carvalho et al.*, 2015].

Because the return stroke channel is a plasma that produces dispersive characteristics in the electromagnetic signals propagating through it and optical signals emitted from it [*Kawasaki et al.*, 1987; *Carvalho et al.*, 2015], *Kawasaki et al.* [1987] defined the return stroke “tip velocity” (presumably the first luminosity above the threshold level) and “group velocity,” observed in a study of luminosity signals measured at two different channel heights for 45 negative triggered lightning return strokes. *Kawasaki et al.* [1987] estimated the average group velocity from the difference between Fourier transform components of two luminosity signals 250 m apart above the triggered lightning conducting wire and found that velocity to be, on average, half the tip velocity, which was calculated by taking the arrival time difference of the separated time domain luminosity signals. In this paper we expand the work of *Kawasaki et al.* [1987] and analyze the dispersion relations of triggered lightning return stroke luminosity measured at four different channel heights. We find the frequency domain transfer function between different pairs of time domain luminosity signals—each measured at a different channel height—and measure the amplitude and phase difference of these transfer functions, which are further used to calculate the upward luminosity return stroke amplitude, phase velocity, and group velocity as a function of signal frequency. Finally, we measure the return stroke velocity in the time domain by using a traditional method (20% of peak amplitude value) and using a cross-correlation technique.

2. Experiment

The experiment described here was performed at the International Center for Lightning Research and Testing in north central Florida in summer 2014 and involved measuring the time domain luminosity of the triggered

lightning return stroke channel at different heights. *Carvalho et al.* [2015] has reported on the experimental setup for flashes triggered on or after 13 August 2014. Briefly, the 11 Thorlabs APD120A2 avalanche photodiode modules, having a 50 MHz -3 dB bandwidth and an optical bandwidth ranging from 200 nm to 1000 nm with a peak response at 600 nm, combined with an adjustable horizontal slit set at 0.51 mm and a neutral density filter with an optical transmission of 10%, were located 205 m from the rocket launcher (depicted in Figure 1 of *Carvalho et al.* [2015]). Both the slit and the filter were located 146 mm in front of the photodiode. Each photodiode was assembled on a Thorlabs lockable rotation platform RP01 with radial scale marked every 2° . All luminosity versus height and time data were measured by using two 4-channel 12-bit LeCroy HDO6054 oscilloscopes having 500 MHz bandwidth and one 4-channel 12-bit LeCroy HRO 64Zi oscilloscope having 400 MHz bandwidth. The sampling rate varied from 500 MHz to 1.25 GHz during recorded 10 ms segments having 20% pretrigger. All photodiodes used in this experiment were tested for linearity by using a strobe source and a series of increasing neutral density filters and exhibited a linear response to input light. A similar experiment setup to that described in *Carvalho et al.* [2015] was used for flashes triggered prior to 13 August 2014, the only difference being a lower number of photodiodes used (7 instead of 11) and a different height distribution. In section 3, we will present the results obtained by using four of the seven photodiode measurements for return strokes triggered prior to 13 August 2014 and by using 4 of the 11 available photodiodes for events on or after 13 August 2014. We choose three channel sections (bottom, middle, and top) so as to optimize the signal-to-noise ratio (SNR) of the analysis. In section 2, to introduce the methodology involved in the analysis, we will analyze in detail the fourth return stroke of UF 14-51 (triggered on 13 August 2014).

3. Method

A time domain signal $x(t)$ can be transformed into a frequency domain signal $X(f)$ by using the Fourier transform defined, for continuous signals, as

$$\mathcal{F}\{x(t)\} = X(f) = \int_{-\infty}^{\infty} x(t)e^{-i2\pi ft} dt \quad (1)$$

where $i = \sqrt{-1}$, f is frequency in hertz, and t is time. The analogous discrete Fourier transform applies to sampled versions of continuous signals can be written in the form [Bergland, 1969]

$$X[k] = \frac{1}{N} \sum_{n=0}^{N-1} x[n]e^{-i2\pi kn/N} \quad (2)$$

$x[n]$ is a finite-length sequence of length N samples for $n=0, 1, \dots, N-1$ and $k=0, 1, \dots, N-1$. $X(f)$ is a complex exponential and can be represented by both magnitude, $|X(f)|$, and phase, $\angle X(f)$, components. Essentially, the frequency domain signal $X(f)$ characterizes the sinusoidal frequency components that comprise the sampled version of the time domain waveform.

The output $y[n]$ of a linear time-invariant (LTI) system that results from an input $x[n]$ can be expressed in the frequency domain as

$$Y(f) = X(f)H(f) \quad (3)$$

or

$$H(f) = \frac{Y(f)}{X(f)} \quad (4)$$

where $X(f)$ and $Y(f)$ are the discrete Fourier transforms of the input and output sequences, respectively. $H(f)$ is called the system transfer function (or frequency response) and is both discrete in frequency and constant for fixed f . Knowing the transfer function characterized by equation (4), we can determine if the system amplifies or attenuates a given sinusoidal component of the input and how much of a phase shift the system adds to that particular sinusoidal component of the input.

With phase specified as a continuous function of f , the phase delay of a system is defined as

$$\tau_p(f) = -\frac{\angle H(f)}{2\pi f} \quad (5)$$

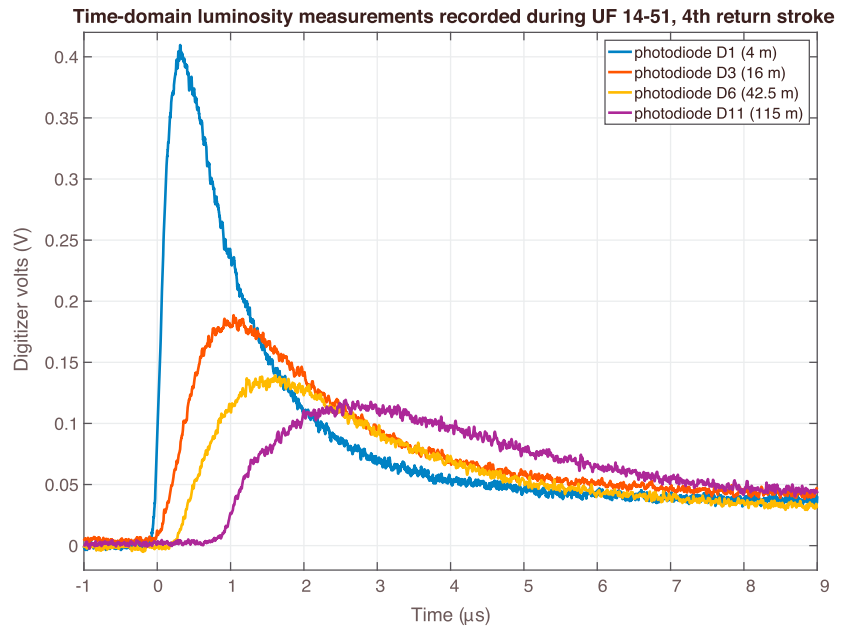


Figure 1. Ten-microsecond time segment of the luminosity waveform recorded by photodiodes D1, D3, D6, and D11 during the fourth return stroke of UF 14-51.

where $\angle H(f)$ is the transfer function phase in radians and f is frequency in hertz. Similarly, the group delay is defined in this context as

$$\tau_g(f) = -\frac{1}{2\pi} \left(\frac{d}{df} \angle H(f) \right) \tag{6}$$

Because $H(f)$ is a complex exponential, the phase delay of each sinusoidal component of the input signal is defined as the *time delay* in seconds between features of each sinusoid measured at different locations [Papoulis, 1977]. In our analysis, the upward luminosity phase velocity can be directly calculated by dividing the channel height difference seen by pairs of diodes by the phase delay given by equation (5). Thus, the upward luminosity phase velocity is given by

$$v_p(f) = \frac{\Delta z}{\tau_p(f)} \tag{7}$$

where $\Delta z = z_2 - z_1$. In addition, the group velocity is similarly defined as

$$v_g(f) = \frac{\Delta z}{\tau_g(f)} \tag{8}$$

Figure 1 shows a 10 μ s time segment of time domain luminosity signals measured at four different channel heights during the fourth return stroke of UF 14-51, adapted from Carvalho *et al.* [2015]. As noted previously, we consider only three sections, i.e., four channel heights, (instead of 10, i.e., 11 photodiodes) of the triggered lightning channel due to SNR limitations. In Figure 1, the curves plotted in blue, red, yellow, and purple represent the luminosity pulse measured by the photodiode D1 (aimed 4 m above the striking point), D3 (16 m), D6 (42.5 m), and D11 (115 m), respectively. Assuming that an LTI system produces the optical emissions shown in Figure 1, the lightning channel is interpreted as a lossy and dispersive medium because the amplitudes of the time domain waveforms decrease with increasing height, while both the 10–90% risetimes and half-width times increase with increasing height.

In order to minimize the impact of noise on the calculations, we begin this methodology by applying a 500 μ s tapered cosine window to two portions of the waveform: one containing the measured luminosity signal and one containing noise preceding the signal. The window is carefully applied to each luminosity signal in such a way that the rolling portion of the window does not affect the rising edge of the waveform. “Applying the window” simply means that the 500 μ s tapered cosine window was multiplied in the time domain to the

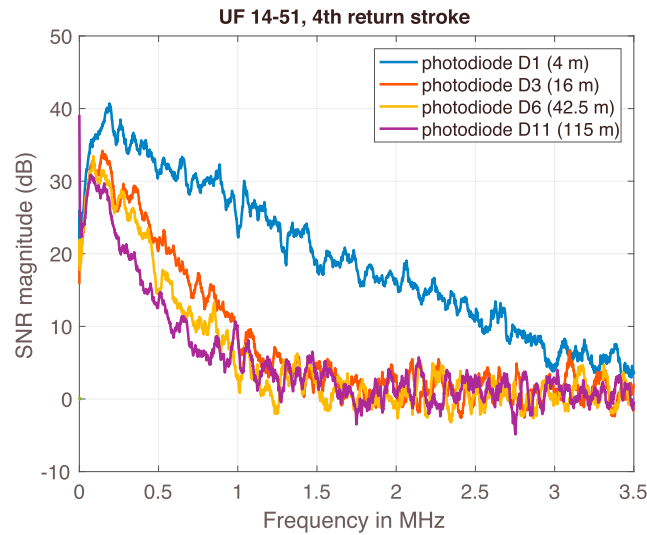


Figure 2. Signal-to-noise ratio (SNR) calculated for photodiodes D1, D3, D6, and D11 as a function of frequency for the fourth return stroke of UF 14-51. The SNR decreases more rapidly for signals recorded by photodiodes aimed at a higher channel altitude.

measured luminosity waveform. We then perform a fast Fourier transform (FFT) to the windowed data and to the corresponding windowed noise in order to calculate the SNR magnitude as a function of frequency for the luminosity data recorded by each photodiode. Dividing the FFT of the windowed data by the FFT of the windowed noise for each photodiode, and then plotting the amplitude in decibel of this ratio, results in the SNR amplitude as a function of frequency for each photodiode. We note that the noise signal present in all luminosity waveforms measured as a function of channel height is effectively constant at all heights since the photodiodes used in this experiment are identical. Figure 2 shows the plot of the SNR amplitude in decibel as a function of frequency for the four diodes considered in this example. We note

that all curves presented in Figure 2 were filtered by using a 5-point moving average filter in order to reduce erratic SNR magnitude variations. It is clear from Figure 2 that the SNR amplitude decreases more rapidly with frequency for photodiodes aimed at higher triggered lightning channel heights, meaning that higher-frequency luminosity components that exist at the bottom of the channel do so to a lesser degree at the top. In section 3, we introduce a detailed table containing the SNR amplitude calculated at different signal frequencies and channel heights.

Because the goal of this paper is to compare luminosity signals up to the highest altitude, i.e., the height seen by D7 for flashes triggered prior to 13 August 2014, and by D11 for flashes triggered on or after that date (both being 115 m), our analysis is only performed for frequency components where the SNR magnitude for the top photodiode is greater than 10 dB, or approximately 300 kHz for the fourth return stroke of UF 14-51.

In the analysis to follow, we relate our time domain luminosity measurements to the discrete Fourier transform presented above and, as an example, arbitrarily select the system input as the signal measured during the fourth return stroke of UF 14-51 by photodiode D6 (aimed at 42.5 m) and the system output as the luminosity signal measured by photodiode D11 (aimed at 115 m), so as to illustrate the main results of this frequency domain analysis. Thus, for this example, $x[n] = \ell_{D6}[n]$ and $y[n] = \ell_{D11}[n]$.

A time domain multiplication corresponds to a convolution in the frequency domain, and therefore, the frequency domain transfer function given in equation (4) becomes, for this example,

$$H_{D6,D11}(f) = \frac{L_{D11}(f) * W(f)}{L_{D6}(f) * W(f)} \tag{9}$$

where $L_{D6}(f)$ represents the FFT of the luminosity waveform measured by photodiode D6 (yellow curve of Figure 1), $L_{D11}(f)$ represents the FFT of the luminosity recorded by photodiode D11 (purple curve of Figure 1), and $W(f)$ represents the FFT of the same time domain window applied to two different signals. We note that $W(f)$ is narrow in frequency (~ 2 kHz), so that the convolutions shown above do not significantly affect the analysis over much larger-frequency ranges.

Equation (9) can be used to directly calculate the transfer function phase as a function of frequency. Due to measurement noise, however, we fit a curve through the calculated transfer function phase and use that curve to characterize the phase progression between pairs of photodiodes. The fit selected was a nonlinear least squares fit weighted by the SNR as a function of frequency, shown in Figure 2 above. In Figure 3a, we

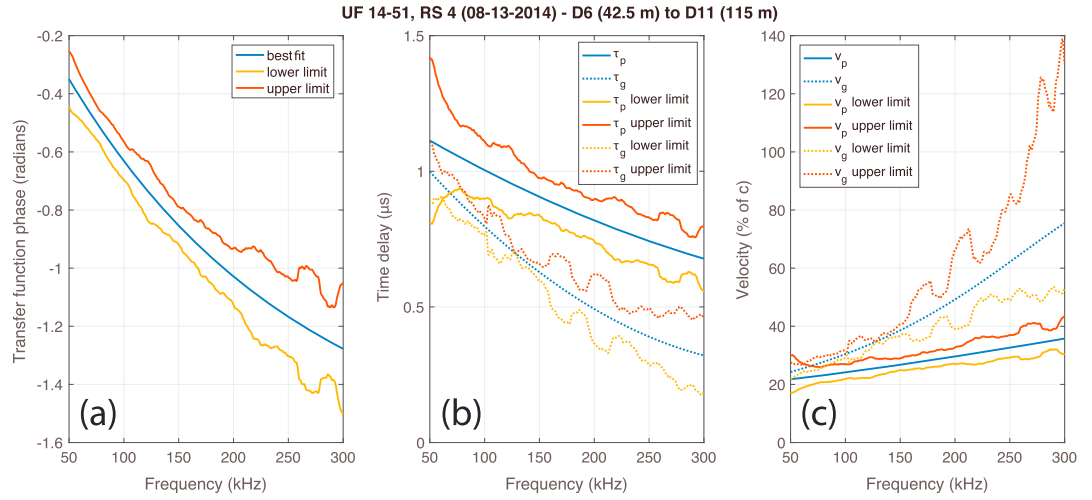


Figure 3. Results from frequency domain analysis for the channel section between 42.5 m and 115 m, recorded during the fourth return stroke of UF 14-51. (a) The transfer function phase fit—weighted by the signal-to-noise ratio (SNR) as a function of frequency—in blue and the lower and upper limits, also found from the SNR. (b) The phase delay along with its lower and upper limits (blue, yellow, and red solid lines, respectively) and the group delay (dotted lines). (c) The phase velocity (solid curves) and group velocity (dotted curves).

plot in blue the resulting transfer function phase fit representing the calculated $\angle H_{D_6, D_{11}}(f)$, modeled after the following analytical form:

$$\Phi(f) = \angle H_{D_6, D_{11}}(f) = p_1 \cdot (2\pi f)^3 + p_2 \cdot (2\pi f)^2 + p_3 \cdot (2\pi f) + p_4 \quad (10)$$

where p_1 , p_2 , p_3 , and p_4 are -5.61×10^{-20} , 4.01×10^{-13} , -1.23×10^{-6} , and -4.21×10^{-12} , respectively, and f is frequency in hertz. The yellow and red lines also plotted in Figure 3a represent the transfer function phase error range, which was also calculated by using the SNR as a function of frequency shown in Figure 2.

Assuming that the third degree polynomial represented by the blue curve in Figure 3a is a good representation of the transfer function phase data, we use equation (5) to find the phase delay ($\tau_p(f)$) between the two channel heights by simply dividing the phase fit given in equation (10) by $\omega = 2\pi f$, or analytically,

$$\tau_p(f) = -\frac{\Phi(f)}{2\pi f} = -p_1 \cdot (2\pi f)^2 - p_2 \cdot (2\pi f) - p_3 - \frac{p_4}{(2\pi f)} \quad (11)$$

Similarly, we use equation (6) to calculate the group delay between the two channel heights, or analytically,

$$\tau_g(f) = -\frac{1}{2\pi} \left(\frac{d}{df} \Phi(f) \right) = -3 \cdot p_1 \cdot (2\pi f)^2 - 2 \cdot p_2 \cdot (2\pi f) - p_3 \quad (12)$$

Equations (11) and (12) are plotted in solid and dotted blue lines, respectively, in Figure 3b, along with the error range calculated by using the SNR as a function of frequency. In Figure 3b, the solid curves represent phase delay results in microseconds and the dotted curves represent the group delay results, also in microseconds. Finally, using equations (7) and (8), we arrive at the two blue curves plotted in Figure 3c, which represent the phase (solid line) and group (dotted line) velocities as a function of frequency for the luminosity signal propagating between heights $z_1 = 42.5$ m and $z_2 = 115$ m. As with Figures 3a and 3b, the red and yellow curves indicate the velocity ranges calculated from the SNR as a function of frequency for both phase (solid line) and group (dotted line) velocities.

4. Results

In order to illustrate the results from the frequency domain analysis described in the previous section, we analyze the fourth return stroke of UF 14-51, following the method described in section 3 for the three channel sections (bottom, middle, and top) considered. This return stroke was selected because there was no evidence of a dart leader in the luminosity versus channel height prior to the return stroke [Carvalho et al., 2015].

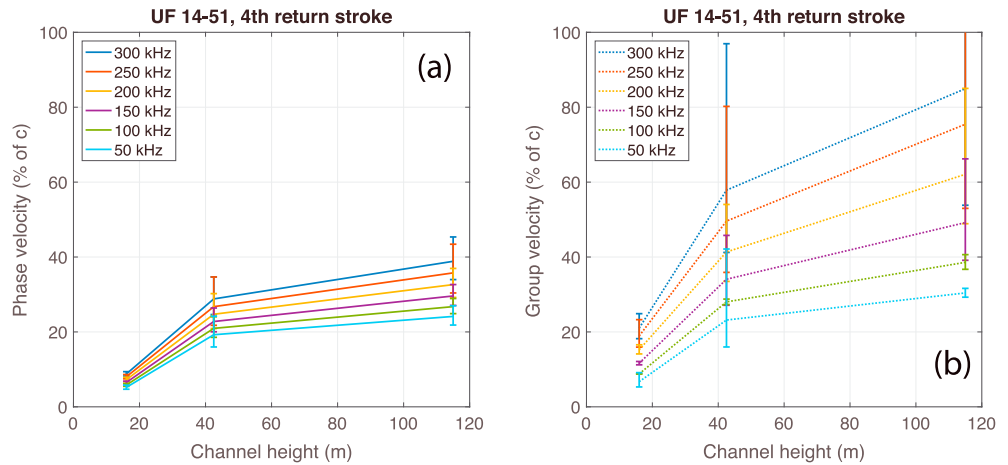


Figure 4. Results calculated from data recorded during the fourth return stroke of UF 14-51. (a) The phase velocity as a function of channel height taken at six different narrowband frequencies ranging from 50 kHz to 300 kHz. The luminosity phase velocity increases with increasing channel height (up to 115 m) and with increasing frequency. Averaged over the three channel sections, the phase velocities calculated at 300 kHz are approximately 64% larger than those calculated at 50 kHz. (b) The group velocity as a function of channel height taken at six different narrowband frequencies ranging from 50 kHz to 300 kHz. The luminosity group velocity increases with increasing channel height (up to 115 m) and with increasing frequency. Averaged over the three channel sections, the group velocities calculated at 300 kHz are approximately 3 times larger than those calculated at 50 kHz. Because the group delay is related to the derivative of a fitted curve, the uncertainty in calculating group velocity is larger than in calculating phase velocity.

Figure 4a shows the phase velocity as a function of triggered lightning channel height taken at six different narrowband frequencies. Each curve shown in Figure 4a was found after following the method described in section 3 for the three channel sections (bottom: D1 (4 m) to D3 (16 m), middle: D3 (16 m) to D6 (42.5 m), and top: D6 (42.5 m) to D11 (115 m)), and then plotting the results for narrowband frequencies ranging from 50 kHz to 300 kHz. The error bars seen in Figures 4a and 4b are simply the ranges plotted in Figure 3c (yellow and red curves) for all channel heights, taken at six narrowband frequencies. Similarly, Figure 4b shows the group velocity as a function of triggered lightning channel height taken at six different narrowband frequencies, also ranging from 50 kHz to 300 kHz. Because the group delay is related to the derivative of a fitted curve, the uncertainty in calculating group velocity is larger than in calculating phase velocity.

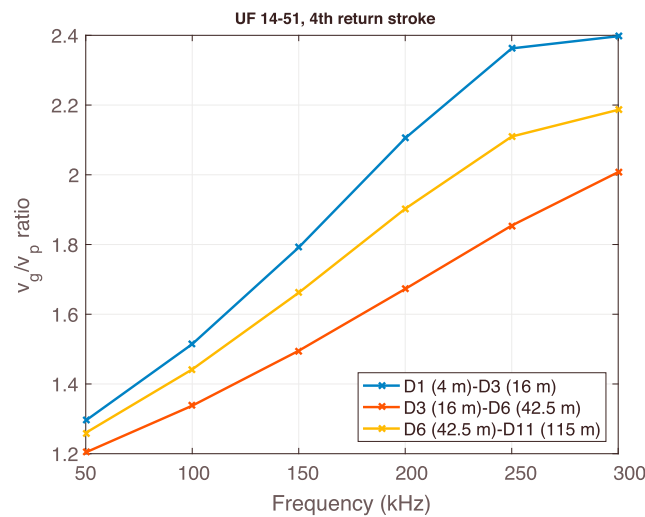


Figure 5. Group velocity to phase velocity ratio as a function of frequency for different channel sections for measurements taken during the fourth return stroke of UF 14-51. At lower frequencies, the v_g/v_p ratio approaches 1, and at higher frequencies it approaches a value of approximately 2.

Consequently, the group velocity error bars seen in Figure 4b are greater than the phase velocity error bars seen in Figure 4a. We note that all curves plotted in Figures 4a and 4b were calculated for the three channel sections (bottom, middle, and top), but we choose to plot the phase and group velocities at the top of each section (i.e., at 16 m, 42.5 m, and 115 m, respectively) for simplicity.

In order to directly compare both group and phase velocities calculated in the frequency domain for the fourth return stroke of UF 14-51, we plot in Figure 5 the v_g/v_p ratio as a function of frequency for the return stroke considered here. Figure 5 shows that for the fourth return stroke of UF 14-51, the group velocity is up to 2.4 times greater than the phase velocity calculated at the same

Table 1. Transfer Function Phase Fit Coefficients

1	2	3	4	5	6	8	9	10	11	12
Date	Event	Return Stroke Number	Input Signal	Output Signal	p1 (Best Fit)	p2 (Best Fit)	p3 (Best Fit)	p4 (Best Fit)	Coefficient of Determination R^2	Mean Square Error
14/7/2014	UF 14-27	1	D1 (4 m)	D2 (32 m)	2.81E-20	-1.72E-14	-4.86E-07	-1.51E-12	0.91	9.E-03
			D2 (32 m)	D4 (65 m)	2.25E-20	5.80E-14	-5.04E-07	-1.43E-12	0.82	7.E-03
			D4 (65 m)	D11 (115 m)	-6.91E-20	3.76E-13	-8.15E-07	-6.05E-12	0.83	7.E-03
14/7/2014	UF 14-27	3	D1 (4 m)	D2 (32 m)	-5.29E-21	2.45E-13	-1.17E-06	-8.82E-13	0.96	8.E-03
			D2 (32 m)	D4 (65 m)	-1.07E-19	5.20E-13	-8.87E-07	-2.78E-12	0.69	7.E-03
			D4 (65 m)	D11 (115 m)	2.04E-21	9.34E-14	-5.18E-07	-1.61E-12	0.88	5.E-03
14/7/2014	UF 14-27	6	D1 (4 m)	D2 (32 m)	-4.89E-20	4.22E-13	-1.39E-06	-3.96E-12	0.94	1.E-02
			D2 (32 m)	D4 (65 m)	-3.42E-20	1.95E-13	-5.27E-07	-1.55E-12	0.56	9.E-03
			D4 (65 m)	D11 (115 m)	-3.41E-20	2.20E-13	-5.86E-07	-1.85E-12	0.80	8.E-03
14/7/2014	UF 14-27	7	D1 (4 m)	D2 (32 m)	-4.70E-20	3.76E-13	-1.18E-06	-3.22E-12	0.91	2.E-02
			D2 (32 m)	D4 (65 m)	-8.47E-20	3.88E-13	-7.78E-07	-2.45E-12	0.81	6.E-03
			D4 (65 m)	D11 (115 m)	1.05E-19	-1.85E-13	-4.17E-07	-1.33E-12	0.89	5.E-03
14/7/2014	UF 14-27	9	D1 (4 m)	D2 (32 m)	-7.97E-20	5.07E-13	-1.35E-06	-3.73E-12	0.96	8.E-03
			D2 (32 m)	D4 (65 m)	-3.50E-20	1.92E-13	-5.49E-07	-1.37E-12	0.80	6.E-03
			D4 (65 m)	D11 (115 m)	-4.33E-20	2.33E-13	-6.14E-07	-1.98E-12	0.89	4.E-03
14/7/2014	UF 14-30	3	D1 (4 m)	D2 (32 m)	-3.63E-20	3.42E-13	-1.36E-06	-3.37E-12	0.99	3.E-03
			D2 (32 m)	D4 (65 m)	-5.03E-20	2.93E-13	-6.35E-07	-1.58E-12	0.94	9.E-04
			D4 (65 m)	D11 (115 m)	1.60E-21	7.76E-14	-4.56E-07	-1.42E-12	0.85	7.E-03
25/7/2014	UF 14-35	2	D1 (4 m)	D3 (16 m)	-3.00E-20	1.55E-13	-4.90E-07	-1.44E-12	0.97	4.E-04
			D3 (16 m)	D6 (42.5 m)	-4.22E-20	4.23E-13	-1.13E-06	-4.10E-12	0.96	3.E-03
			D6 (42.5 m)	D11 (115 m)	1.78E-19	-1.39E-13	-7.86E-07	-5.26E-12	0.94	3.E-03
25/7/2014	UF 14-35	4 ^b	D1 (4 m)	D3 (16 m)	-1.79E-20	1.21E-13	-2.61E-07	-6.00E-13	0.79	7.E-04
			D3 (16 m)	D6 (42.5 m)	-3.45E-20	3.06E-13	-8.57E-07	-2.71E-12	0.71	2.E-02
			D6 (42.5 m)	D11 (115 m)	-5.61E-20	4.01E-13	-1.23E-06	-4.21E-12	0.97	3.E-03
13/8/2014	UF 14-51	4	D1 (4 m)	D3 (16 m)	-5.09E-20	3.45E-13	-9.70E-07	-2.22E-12	0.95	6.E-03
			D3 (16 m)	D6 (42.5 m)	-1.72E-20	1.46E-13	-5.45E-07	-1.42E-12	0.82	1.E-02
			D6 (42.5 m)	D11 (115 m)	-5.61E-20	4.01E-13	-1.23E-06	-4.21E-12	0.89	3.E-02
13/8/2014	UF 14-51	6	D1 (4 m)	D3 (16 m)	-4.39E-20	3.25E-13	-9.67E-07	-2.00E-12	0.93	7.E-03
			D3 (16 m)	D6 (42.5 m)	-1.98E-20	2.01E-13	-6.92E-07	-1.88E-12	0.59	3.E-02
			D6 (42.5 m)	D11 (115 m)	-9.16E-20	6.73E-13	-1.62E-06	-6.89E-12	0.91	1.E-02
14/8/2014	UF 14-52	2 ^{ab}	D1 (4 m)	D3 (16 m)	-5.01E-21	4.54E-14	-1.56E-07	-3.61E-13	0.90	4.E-04
			D3 (16 m)	D6 (42.5 m)	-1.39E-20	1.02E-13	-4.51E-07	-1.13E-12	0.99	9.E-04
			D6 (42.5 m)	D11 (115 m)	4.40E-20	1.94E-13	-1.25E-06	-4.28E-12	0.99	2.E-03
14/8/2014	UF 14-52	5	D1 (4 m)	D3 (16 m)	-2.28E-20	1.90E-13	-7.33E-07	-1.72E-12	0.99	1.E-03
			D3 (16 m)	D6 (42.5 m)	-6.51E-20	4.08E-13	-9.33E-07	-2.56E-12	0.78	1.E-02
			D6 (42.5 m)	D11 (115 m)	-7.43E-20	4.11E-13	-1.04E-06	-3.27E-12	0.74	4.E-02
			Average (μ)		-2.60E-20	2.51E-13	-8.21E-07	-2.57E-12	0.87	9.E-03
			Median		-3.45E-20	2.45E-13	-7.86E-07	-2.00E-12	0.89	7.E-03
		Standard deviation (σ)			5.34E-20	1.83E-13	3.59E-07	1.53E-12	0.11	9.E-03

^aSmall dart leader appears in signal D11.

^bVelocity reduces with height.

frequency. Figure 5 also shows that for increasing signal frequency, the v_g/v_p ratio increases for a constant channel segment, indicating that the group velocity may approach the phase velocity value at lower frequency components.

Following the same approach described above, we analyze 11 additional return strokes in order to assess the variability of our results. The second return stroke of UF 14-52 is the only stroke with evidence of a small dart leader preceding the return stroke rise, but it likely does not affect the conclusions significantly. Therefore, except for one case, our main data set consists of return stroke luminosity profiles with no evidence of a luminous dart leader. Clearly, there had to be a dart leader preceding each return stroke and likely an upward leader of a few meters in length connecting to the downward dart leader above the triggering structure [Wang et al., 1999]. Further, the fact that the return stroke must start at the connection point and travel both upward and downward from that point could influence the measured results for the lowest channel section observed.

Table 2. Signal-to-Noise Amplitude Luminosity Signal Components as a Function of Channel Height and Frequency in Linear Units (Amplitude Values in Decibels Were Transformed Into Unit-Less Values by Using the Inverted Logarithm Detailed in the Text)^a

1	2	3	4	5	6	7	8	9	10
Date	Event	Return Stroke Number	Photodiode	SNR Amplitude Ratio at 100 kHz	SNR Amplitude Ratio at 200 kHz	SNR Amplitude Ratio at 300 kHz	SNR Amplitude Ratio at 400 kHz	SNR Amplitude Ratio at 500 kHz	SNR Amplitude Ratio at 600 kHz
14/7/2014	UF 14-27	1	D1 (4 m)	116.3	112.6	147.7	48.0	38.6	23.3
			D2 (32 m)	46.9	18.7	8.9	7.2	2.8	4.1
			D4 (65 m)	41.4	13.1	9.1	4.5	2.2	2.0
			D7 (115 m)	40.8	27.6	7.6	7.9	3.1	3.6
14/7/2014	UF 14-27	3	D1 (4 m)	141.6	420.1	161.2	189.7	135.8	167.3
			D2 (32 m)	25.9	23.9	11.2	9.4	2.7	6.3
			D4 (65 m)	33.2	15.6	5.6	5.3	2.1	1.7
			D7 (115 m)	48.7	42.0	15.9	8.2	2.7	1.5
14/7/2014	UF 14-27	6	D1 (4 m)	725.4	282.4	150.3	457.5	185.5	106.1
			D2 (32 m)	19.8	24.8	13.3	6.2	2.4	3.4
			D4 (65 m)	19.7	19.7	5.2	9.1	1.5	1.8
			D7 (115 m)	49.0	32.2	10.0	8.8	2.8	2.1
14/7/2014	UF 14-27	7	D1 (4 m)	162.7	184.5	121.2	145.5	74.4	45.9
			D2 (32 m)	46.3	26.7	14.4	7.8	4.0	4.3
			D4 (65 m)	18.2	12.9	20.0	3.0	3.4	2.3
			D7 (115 m)	91.5	43.0	25.5	9.3	5.0	9.9
14/7/2014	UF 14-27	9	D1 (4 m)	244.0	199.4	293.8	296.9	128.1	119.4
			D2 (32 m)	36.6	17.2	26.0	7.3	2.6	5.3
			D4 (65 m)	18.9	12.8	18.1	9.0	5.3	1.9
			D7 (115 m)	72.4	35.4	17.0	8.5	8.0	4.3
14/7/2014	UF 14-30	3	D1 (4 m)	141.7	214.1	172.7	172.7	86.5	132.2
			D2 (32 m)	142.9	88.9	70.5	48.7	15.3	20.5
			D4 (65 m)	84.3	159.0	44.9	21.6	12.8	8.4
			D7 (115 m)	170.0	90.1	21.9	17.3	9.0	7.7
25/7/2014	UF 14-35	2	D1 (4 m)	110.4	125.4	91.3	101.5	54.9	71.5
			D3 (16 m)	116.3	112.6	71.9	52.0	34.1	25.6
			D6 (42.5 m)	77.5	64.5	26.5	11.9	7.6	5.0
			D11 (115 m)	44.6	15.8	5.8	4.1	1.6	1.7
25/7/2014	UF 14-35	4 ^b	D1 (4 m)	66.2	30.6	18.0	16.8	6.5	5.6
			D3 (16 m)	44.6	15.8	5.8	4.1	1.6	1.7
			D6 (42.5 m)	79.5	63.8	50.5	38.3	27.2	29.2
			D11 (115 m)	51.1	65.2	61.1	28.4	21.5	12.9
13/8/2014	UF 14-51	4	D1 (4 m)	58.8	67.8	50.6	42.9	35.0	26.9
			D3 (16 m)	46.4	37.1	32.0	15.0	11.1	8.9
			D6 (42.5 m)	56.0	26.5	26.3	17.1	4.8	6.2
			D11 (115 m)	22.0	23.1	11.3	8.7	4.9	2.7
13/8/2014	UF 14-51	6	D1 (4 m)	62.4	85.4	97.7	69.3	40.2	48.4
			D3 (16 m)	28.9	24.8	21.1	17.7	8.9	7.1
			D6 (42.5 m)	34.9	20.3	12.9	10.1	4.1	3.6
			D11 (115 m)	21.1	12.3	5.2	5.0	2.0	1.8
14/8/2014	UF 14-52	2 ^{bc}	D1 (4 m)	328.3	200.7	157.2	104.8	68.1	62.4
			D3 (16 m)	209.2	185.0	114.6	107.8	86.0	49.9
			D6 (42.5 m)	151.4	132.8	65.8	48.1	32.5	22.0
			D11 (115 m)	148.6	117.2	28.2	28.0	11.8	11.4
14/8/2014	UF 14-52	5	D1 (4 m)	208.5	527.1	273.8	145.4	91.6	147.0
			D3 (16 m)	206.8	238.1	113.4	114.6	40.2	32.7
			D6 (42.5 m)	201.3	63.7	69.1	65.2	12.1	15.4
			D11 (115 m)	184.1	70.9	49.8	18.6	13.9	10.4

^a ΔR represents the change in the amplitude of a selected frequency component as a function of height.

^bVelocity reduces with height.

^cSmall dart leader appears in signal D11.

Table 2. (continued)

11	12	13	14	15	16	17	18	19	20
SNR Amplitude Ratio at 700 kHz	SNR Amplitude Ratio at 800 kHz	SNR Amplitude Ratio at 900 kHz	SNR Amplitude Ratio at 1 MHz	ΔR at 100 kHz	ΔR at 200 kHz	ΔR at 300 kHz	Percentage Difference of ΔR at 100 kHz	Percentage Difference of ΔR at 200 kHz	Percentage Difference of ΔR at 300 kHz
19.5	28.2	16.1	14.0						
2.5	1.9	2.3	1.0	-69.4	-93.9	-138.8	-60%	-83%	-94%
4.3	0.9	1.2	0.8	-5.5	-5.6	0.2	-12%	-30%	2%
3.6	1.1	0.9	1.2	-0.6	14.5	-1.5	-1%	111%	-17%
128.2	95.5	37.6	41.5						
5.6	1.7	1.7	1.3	-115.7	-396.2	-150.0	-82%	-94%	-93%
1.7	1.9	0.6	0.6	7.3	-8.3	-5.6	28%	-35%	-50%
4.3	3.1	2.3	0.6	15.5	26.4	10.3	47%	170%	186%
97.2	70.3	98.1	48.7						
2.5	0.8	1.5	1.7	-705.6	-257.7	-136.9	-97%	-91%	-91%
0.6	1.1	1.7	0.8	-0.2	-5.1	-8.1	-1%	-20%	-61%
2.1	1.7	3.4	1.2	29.4	12.5	4.8	149%	63%	93%
57.7	54.0	43.9	103.5						
2.7	2.0	2.4	0.5	-116.4	-157.8	-106.7	-72%	-86%	-88%
1.1	0.9	1.1	1.8	-28.1	-13.8	5.6	-61%	-52%	39%
3.5	2.1	1.9	1.0	73.3	30.1	5.5	402%	234%	27%
91.1	77.8	143.4	35.3						
3.2	1.2	1.1	1.7	-207.5	-182.2	-267.7	-85%	-91%	-91%
1.3	1.8	1.9	1.3	-17.7	-4.4	-7.9	-48%	-26%	-30%
9.2	3.7	4.1	1.1	53.6	22.6	-1.1	284%	177%	-6%
97.8	70.3	81.4	61.8						
10.8	25.8	5.0	2.1	1.2	-125.3	-102.2	1%	-59%	-59%
4.0	4.4	3.5	3.7	-58.6	70.2	-25.6	-41%	79%	-36%
6.1	5.7	7.8	2.3	85.7	-69.0	-23.0	102%	-43%	-51%
			Average (μ)	-58.8	-63.5	-52.7	25%	7%	-23%
			Median	-3.1	-7.0	-8.0	-7%	-32%	-43%
			Standard deviation (σ)	176.8	120.3	78.8	134%	105%	74%
53.7	42.3	28.5	25.8						
20.7	20.2	18.0	12.6	5.9	-12.8	-19.3	5%	-10%	-21%
3.3	4.2	2.8	1.6	-38.8	-48.1	-45.4	-33%	-43%	-63%
1.5	1.0	1.7	0.8	-32.9	-48.7	-20.7	-42%	-75%	-78%
3.4	4.3	2.0	2.1						
1.5	1.0	1.7	0.8	-21.6	-14.8	-12.2	-33%	-48%	-68%
13.5	12.6	15.7	7.5	34.9	48.0	44.7	78%	304%	764%
10.5	12.2	6.3	4.4	-28.5	1.4	10.6	-36%	2%	21%
24.4	36.7	33.4	17.7						
6.1	4.1	5.8	3.3	-12.3	-30.7	-18.7	-21%	-45%	-37%
4.8	2.3	2.2	0.9	9.5	-10.6	-5.7	20%	-28%	-18%
3.2	1.7	2.3	4.5	-34.0	-3.4	-14.9	-61%	-13%	-57%
36.1	31.0	25.2	22.4						
4.6	5.8	4.3	2.1	-33.4	-60.6	-76.7	-54%	-71%	-78%
3.9	1.7	1.5	1.4	6.0	-4.5	-8.2	21%	-18%	-39%
2.4	2.1	1.3	1.1	-13.7	-8.0	-7.7	-39%	-39%	-59%
57.2	26.0	29.9	14.7						
34.9	22.3	19.9	16.0	-119.1	-15.7	-42.5	-36%	-8%	-27%
25.3	14.2	14.9	6.3	-57.8	-52.2	-48.9	-28%	-28%	-43%
8.5	3.4	6.3	2.6	-2.8	-15.6	-37.6	-2%	-12%	-57%
122.9	81.8	79.7	45.9						
34.3	25.9	9.7	8.1	-1.7	-288.9	-160.4	-1%	-55%	-59%
6.1	3.2	4.9	3.0	-5.6	-174.4	-44.3	-3%	-73%	-39%
6.0	5.0	3.9	3.2	-17.2	7.2	-19.3	-9%	11%	-28%
			Average (μ)	-20.2	-40.7	-29.3	-15%	-14%	1%
			Median	-15.5	-15.2	-19.3	-24%	-28%	-41%
			Standard deviation (σ)	32.9	76.5	42.0	33%	83%	192%

Table 3. Phase (v_p) and Group (v_g) Velocities Calculated as a Function of Triggered Lightning Channel Height for Selected Narrowband Signal Frequencies From 12 Triggered Lightning Return Strokes, as Well as Two Types of Time Domain Velocity Calculations

1	2	3	4	5	6	7	8	9	10	11	12
Date	Event	Return Stroke Number	Channel Height Section (m)	v_p 50 kHz (m/s)	v_p 100 kHz (m/s)	v_p 150 kHz (m/s)	v_p 200 kHz (m/s)	v_p 250 kHz (m/s)	v_p 300 kHz (m/s)	Average v_p Error (Lower Limit, Upper Limit) (%)	v_g 50 kHz (m/s)
14/7/2014	UF 14-27	1	4 to 32	5.73E+07	5.77E+07	5.87E+07	6.05E+07	6.31E+07	6.69E+07	[-12, 18]	
			32 to 65		7.19E+07	7.68E+07	8.33E+07	9.22E+07		[-18, 29]	
			65 to 115		8.25E+07	9.58E+07	1.11E+08	1.27E+08		[-18, 28]	
14/7/2014	UF 14-27	3	4 to 32	2.57E+07	2.76E+07	2.98E+07	3.23E+07	3.53E+07	3.87E+07	[-7, 8]	2.76E+07
			32 to 65	4.49E+07	5.47E+07	6.71E+07	8.20E+07			[-19, 34]	
			65 to 115		1.09E+08	1.17E+08	1.26E+08	1.37E+08		[-17, 27]	
14/7/2014	UF 14-27	6	4 to 32	2.21E+07	2.44E+07	2.69E+07	2.97E+07	3.29E+07	3.62E+07	[-6, 7]	2.45E+07
			32 to 65			8.84E+07	9.84E+07			[-21, 37]	
			65 to 115		1.08E+08	1.22E+08	1.38E+08	1.54E+08		[-20, 35]	
14/7/2014	UF 14-27	7	4 to 32	2.64E+07	2.92E+07	3.25E+07	3.60E+07	3.99E+07	4.42E+07	[-8, 10]	
			32 to 65		5.82E+07	6.77E+07	7.78E+07	8.75E+07	9.50E+07	[-19, 33]	
			65 to 115		1.02E+08	1.01E+08	1.04E+08	1.12E+08	1.28E+08	[-18, 29]	
14/7/2014	UF 14-27	9	4 to 32	2.33E+07	2.62E+07	2.96E+07	3.32E+07	3.71E+07	4.11E+07	[-6, 8]	2.64E+07
			32 to 65		7.46E+07	8.26E+07	9.09E+07	9.88E+07	1.06E+08	[-20, 34]	
			65 to 115		1.03E+08	1.16E+08	1.28E+08	1.41E+08	1.52E+08	[-18, 28]	
14/7/2014	UF 14-30	3	4 to 32	2.24E+07	2.43E+07	2.63E+07	2.85E+07	3.09E+07	3.34E+07	[-2, 3]	2.43E+07
			32 to 65	6.02E+07	7.01E+07	8.18E+07	9.44E+07	1.08E+08	1.22E+08	[-7, 9]	7.08E+07
			65 to 115	1.16E+08	1.23E+08	1.31E+08	1.40E+08	1.51E+08	1.64E+08	[-8, 10]	1.23E+08
			Average (μ)	4.42E+07	6.74E+07	7.50E+07	8.30E+07	9.05E+07	8.56E+07	[-14, 22]	5.43E+07
			Median	2.64E+07	7.01E+07	7.93E+07	8.71E+07	9.55E+07	8.10E+07	[-18, 28]	2.76E+07
			Standard deviation (σ)	3.08E+07	3.36E+07	3.52E+07	3.87E+07	4.52E+07	4.82E+07	[-6, 12]	3.89E+07
25/7/2014	UF 14-35	2	4 to 16	2.70E+07	2.97E+07	3.24E+07	3.51E+07	3.74E+07	3.96E+07	[-7, 10]	2.99E+07
			16 to 42.5	2.64E+07	3.00E+07	3.43E+07	3.96E+07	4.62E+07	5.36E+07	[-7, 8]	3.01E+07
			42.5 to 115	8.92E+07	9.02E+07	9.55E+07	1.07E+08	1.25E+08	1.57E+08	[-14, 22]	8.83E+07
25/7/2014	UF 14-35	4 ^b	4 to 16		6.18E+07	7.37E+07	8.82E+07	1.05E+08	1.25E+08	[-19, 31]	
			16 to 42.5	3.48E+07	3.91E+07	4.42E+07	5.02E+07	5.74E+07	6.60E+07	[-11, 15]	3.93E+07
			42.5 to 115	8.83E+07	6.42E+07	6.05E+07	7.06E+07	1.18E+08		[-12, 16]	5.81E+07
13/8/2014	UF 14-51	4	4 to 16	1.39E+07	1.56E+07	1.74E+07	1.94E+07	2.16E+07	2.39E+07	[-10, 13]	1.57E+07
			16 to 42.5	5.16E+07	5.65E+07	6.19E+07	6.77E+07	7.40E+07	8.06E+07	[-18, 36]	5.67E+07
			42.5 to 115	6.53E+07	7.24E+07	8.02E+07	8.87E+07	9.76E+07	1.07E+08	[-12, 17]	7.28E+07
13/8/2014	UF 14-51	6	4 to 16	1.38E+07	1.54E+07	1.71E+07	1.91E+07	2.12E+07	2.35E+07	[-11, 16]	1.54E+07
			16 to 42.5		4.62E+07	5.10E+07	5.64E+07	6.24E+07	6.90E+07	[-18, 31]	4.64E+07
			42.5 to 115	5.11E+07	5.87E+07	6.80E+07	7.92E+07	9.17E+07	1.06E+08	[-16, 27]	5.91E+07
14/8/2014	UF 14-52	2 ^{ab}	4 to 16	8.41E+07	9.27E+07	1.02E+08	1.13E+08	1.25E+08	1.37E+08	[-13, 21]	9.31E+07
			16 to 42.5	6.30E+07	6.75E+07	7.21E+07	7.68E+07	8.15E+07	8.60E+07	[-6, 7]	6.77E+07
			42.5 to 115	6.06E+07	6.50E+07	7.05E+07	7.72E+07	8.61E+07	9.89E+07	[-3, 3]	6.49E+07
14/8/2014	UF 14-52	5	4 to 16	1.78E+07	1.93E+07	2.09E+07	2.26E+07	2.44E+07	2.63E+07	[-3, 3]	1.93E+07
			16 to 42.5	3.26E+07	3.77E+07	4.36E+07	5.05E+07	5.84E+07	6.68E+07	[-5, 6]	3.80E+07
			42.5 to 115	7.93E+07	8.98E+07	1.01E+08	1.14E+08	1.26E+08	1.38E+08	[-5, 6]	9.06E+07
			Average (μ)	4.99E+07	5.29E+07	5.82E+07	6.53E+07	7.55E+07	8.26E+07	[-11, 16]	5.21E+07
			Median	5.13E+07	5.76E+07	6.12E+07	6.92E+07	7.77E+07	8.06E+07	[-11, 16]	5.67E+07
			Standard deviation (σ)	2.69E+07	2.52E+07	2.75E+07	3.08E+07	3.64E+07	4.20E+07	[-5, 10]	2.57E+07

^aSmall dart leader appears in signal D11.

^bVelocity reduces with height.

Table 1 shows the phase fit coefficients (p_1 , p_2 , p_3 , and p_4 of equation (10)) calculated for the three channel sections (bottom, middle, and top) of each one of the 12 return strokes analyzed in this paper. For these 36 fits (three channel sections times 12 return strokes), the R^2 average value is 0.87, with 0.89 median and average mean square error value of 9×10^{-3} , indicating that the weighted phase fits described in section 2 statistically represent the measured transfer function phase of equation (9) satisfactorily.

Table 3. (continued)

13	14	15	16	17	18	19	20	21	22
v_g 100 kHz (m/s)	v_g 150 kHz (m/s)	v_g 200 kHz (m/s)	v_g 250 kHz (m/s)	v_g 300 kHz (m/s)	Average v_g Error (Lower Limit, Upper Limit) (%)	Time Delay at the 20% Amplitude Level (s)	20% Amplitude Level Time Domain Velocity (m/s)	Δt_{lag} (s)	Cross-Correlation Time Domain Velocity (m/s)
5.90E+07	6.31E+07	7.07E+07	8.44E+07		[-13, 23]	2.20E-07	1.27E+08	-3.54E-07	7.91E+07
8.15E+07	9.85E+07	1.31E+08			[-13, 21]	2.10E-07	1.57E+08	-4.46E-07	7.40E+07
1.18E+08	1.73E+08	2.55E+08			[-10, 19]	3.28E-07	1.52E+08	-4.30E-07	1.16E+08
3.24E+07	3.90E+07	4.87E+07	6.43E+07	9.37E+07	[-13, 19]	3.06E-07	9.15E+07	-6.90E-07	4.06E+07
9.16E+07	1.72E+08				[-11, 18]	2.78E-07	1.19E+08	-5.10E-07	6.47E+07
1.26E+08	1.49E+08				[-8, 10]	3.02E-07	1.66E+08	-3.90E-07	1.28E+08
3.04E+07	3.84E+07	4.95E+07	6.50E+07	8.62E+07	[-17, 37]	3.84E-07	7.29E+07	-8.12E-07	3.45E+07
1.02E+08					[-3, 3]	2.70E-07	1.22E+08	-3.34E-07	9.88E+07
1.43E+08	1.91E+08	2.56E+08			[-16, 29]	2.46E-07	2.03E+08	-3.80E-07	1.32E+08
3.69E+07	4.73E+07	6.17E+07	8.17E+07		[-10, 17]	2.98E-07	9.40E+07	-6.50E-07	4.31E+07
8.45E+07					[-3, 3]	2.54E-07	1.30E+08	-4.22E-07	7.82E+07
9.54E+07	1.03E+08				[-12, 21]	3.14E-07	1.59E+08	-4.28E-07	1.17E+08
3.45E+07	4.58E+07	6.12E+07	7.98E+07	9.61E+07	[-12, 22]	3.10E-07	9.03E+07	-7.32E-07	3.83E+07
9.44E+07	1.18E+08	1.42E+08	1.61E+08		[-19, 30]	2.50E-07	1.32E+08	-4.32E-07	7.64E+07
1.34E+08	1.72E+08	2.14E+08	2.47E+08		[-17, 27]	3.12E-07	1.60E+08	-4.12E-07	1.21E+08
2.89E+07	3.47E+07	4.20E+07	5.11E+07	6.20E+07	[-5, 5]	3.50E-07	8.00E+07	-8.22E-07	3.41E+07
1.01E+08	1.52E+08				[-10, 16]	1.82E-07	1.81E+08	-3.30E-07	1.00E+08
1.40E+08	1.63E+08	1.97E+08	2.49E+08		[-18, 39]	2.64E-07	1.89E+08	-3.48E-07	1.44E+08
8.52E+07	1.10E+08	1.27E+08	1.20E+08	8.45E+07	[-12, 20]	2.82E-07	1.35E+08	-4.96E-07	8.44E+07
9.30E+07	1.10E+08	1.01E+08	8.17E+07	9.00E+07	[-12, 20]	2.88E-07	1.31E+08	-4.29E-07	7.86E+07
3.97E+07	5.81E+07	8.35E+07	7.88E+07	1.56E+07	[-5, 10]	5.07E-08	3.89E+07	1.67E-07	3.67E+07
3.63E+07	4.33E+07	4.96E+07	5.49E+07	5.85E+07	[-9, 13]	1.62E-07	7.39E+07	-2.70E-07	4.45E+07
4.06E+07	5.91E+07	9.82E+07			[-5, 7]	2.42E-07	1.09E+08	-6.19E-07	4.28E+07
9.67E+07	1.26E+08				[-9, 13]	4.90E-07	1.48E+08	-6.19E-07	1.17E+08
9.44E+07	1.58E+08	3.14E+08			[-10, 13]	2.16E-08	5.56E+08	-7.04E-08	1.70E+08
5.14E+07	7.08E+07	1.06E+08			[-11, 21]	2.15E-07	1.23E+08	-4.89E-07	5.42E+07
4.81E+07	6.94E+07				[-4, 5]	5.57E-07	1.30E+08	-7.33E-07	9.89E+07
2.00E+07	2.61E+07	3.44E+07	4.51E+07	5.69E+07	[-13, 22]	1.66E-07	7.23E+07	-4.38E-07	2.74E+07
6.90E+07	8.49E+07	1.05E+08	1.31E+08	1.62E+08	[-15, 26]	2.36E-07	1.12E+08	-3.08E-07	8.60E+07
9.11E+07	1.15E+08	1.46E+08	1.84E+08	2.21E+08	[-12, 20]	5.78E-07	1.25E+08	-8.42E-07	8.61E+07
1.96E+07	2.55E+07	3.35E+07	4.42E+07	5.67E+07	[-10, 15]	1.32E-07	9.09E+07	-4.38E-07	2.74E+07
5.75E+07	7.28E+07	9.45E+07	1.26E+08	1.73E+08	[-20, 36]	2.42E-07	1.10E+08	-4.30E-07	6.16E+07
8.23E+07	1.23E+08	2.08E+08			[12, 26]	7.42E-07	9.77E+07	-9.88E-07	7.34E+07
1.15E+08	1.45E+08	1.87E+08	2.43E+08	3.18E+08	[-16, 26]	3.20E-08	3.75E+08	-8.20E-08	1.46E+08
7.80E+07	8.96E+07	1.02E+08	1.14E+08	1.24E+08	[-9, 13]	1.70E-07	1.56E+08	-3.14E-07	8.44E+07
7.65E+07	9.47E+07	1.26E+08	2.26E+08		[-5, 6]	5.42E-07	1.34E+08	-9.24E-07	7.85E+07
2.30E+07	2.75E+07	3.29E+07	3.92E+07	4.59E+07	[-4, 5]	1.78E-07	6.74E+07	-4.26E-07	2.82E+07
5.31E+07	7.82E+07	1.22E+08	1.96E+08	2.92E+08	[-9, 12]	2.08E-07	1.27E+08	-4.26E-07	6.22E+07
1.19E+08	1.58E+08	2.04E+08	2.46E+08	2.61E+08	[-10, 15]	4.92E-07	1.47E+08	-7.10E-07	1.02E+08
6.51E+07	8.71E+07	1.23E+08	1.37E+08	1.61E+08	[-10, 16]	3.00E-07	1.53E+08	-5.07E-07	7.73E+07
6.32E+07	8.15E+07	1.06E+08	1.29E+08	1.62E+08	[-10, 14]	2.26E-07	1.24E+08	-4.38E-07	7.59E+07
3.12E+07	4.32E+07	7.60E+07	8.02E+07	1.01E+08	[-4, 9]	2.09E-07	1.21E+08	2.62E-07	3.99E+07

In Table 2, we present the SNR amplitude calculated at 10 narrowband signal frequencies (columns 5 to 14) and four heights by applying the same method used to plot Figure 2. As mentioned before, because the noise signal is effectively the same for all photodiodes, a change in SNR calculated at a particular signal frequency for two different channel heights is the equivalent of a change in the amplitude (ΔR) of that frequency component as a function of height. We note that the values shown in Table 2 were converted from decibels to a linear scale using the inverse logarithm expression, or $SNR = 10^{\frac{\text{value in dB}}{20}}$. In columns 15 to 17, we calculate the amplitude change (ΔR) between different channel heights at 100 kHz, 200 kHz, and 300 kHz, respectively. In columns 18 to 20, we calculate the percentage difference of ΔR between different channel heights at 100 kHz, 200 kHz, and 300 kHz, respectively. The statistics provided in Table 2

Table 4. Phase (v_p) and Group (v_g) Velocities (Averaged Over Six Return Strokes Triggered Before 13 August 2014 and Six Return Strokes Triggered on or After That Date) for Each Triggered Lightning Channel Height Section and Narrowband Signal Frequency Components^a

Channel Height Section ^b (m)	2	3	4	5	6	7	8	9	10	11	12	13	14	15
	Average v_p 50 kHz (m/s)	Average v_p 100 kHz (m/s)	Average v_p 150 kHz (m/s)	Average v_p 200 kHz (m/s)	Average v_p 250 kHz (m/s)	Average v_p 300 kHz (m/s)	Average v_p Error (Lower Limit, Upper Limit) (%)	Average v_g 50 kHz (m/s)	Average v_g 100 kHz (m/s)	Average v_g 150 kHz (m/s)	Average v_g 200 kHz (m/s)	Average v_g 250 kHz (m/s)	Average v_g 300 kHz (m/s)	Average v_g Error (Lower Limit, Upper Limit) (%)
4 to 32	2.95E+07	3.16E+07	3.40E+07	3.67E+07	3.99E+07	4.34E+07	[-6, 9]	2.57E+07	3.70E+07	4.47E+07	5.56E+07	7.10E+07	8.45E+07	[-12, 21]
32 to 65	5.26E+07	6.59E+07	7.74E+07	8.78E+07	9.66E+07	1.08E+08	[-17, 29]	7.08E+07	9.26E+07	1.35E+08	1.36E+08	1.61E+08	1.61E+08	[-10, 15]
65 to 115	1.16E+08	1.05E+08	1.14E+08	1.24E+08	1.37E+08	1.48E+08	[-17, 26]	1.03E+08	1.26E+08	1.58E+08	2.30E+08	2.48E+08	2.48E+08	[-14, 24]
4 to 16	3.13E+07	3.91E+07	4.40E+07	4.96E+07	5.58E+07	6.25E+07	[-11, 16]	3.47E+07	5.14E+07	7.10E+07	1.08E+08	8.53E+07	1.07E+08	[-10, 16]
16 to 42.5	4.17E+07	4.62E+07	5.12E+07	5.69E+07	6.33E+07	7.03E+07	[-11, 17]	4.64E+07	5.83E+07	7.59E+07	1.05E+08	1.42E+08	1.88E+08	[-12, 19]
42.5 to 115	7.23E+07	7.34E+07	7.93E+07	8.94E+07	1.07E+08	1.21E+08	[-10, 15]	7.23E+07	8.57E+07	1.14E+08	1.71E+08	2.19E+08	2.41E+08	[-9, 14]

^aData extracted from Table 3.

^bThe first to third rows (4 to 32, 32 to 65, and 65 to 115) are for events triggered before 13 August 2014 and the fourth to sixth rows (4 to 16, 16 to 42.5, and 42.5 to 115) are for events triggered on or after 13 August 2014.

are calculated separately for the two individual data sets: one consisting of flashes triggered prior to 13 August 2014 (UF 14-27 and UF 14-30) and one consisting of flashes triggered on or after that date (UF14-35, UF 14-51, and UF 14-52). The median of the percentage difference of ΔR averaged over all channel heights (seen at the bottom of each section of Table 2) at 100 kHz, 200 kHz, and 300 kHz decreases monotonically with increasing signal frequency. For the flashes triggered prior to 13 August 2014, the amplitude of the 300 kHz luminosity component averaged over all height intervals experiences a decrease of approximately 43%, the amplitude of the 200 kHz component experiences a decrease of 32%, and the amplitude of the 100 kHz component experiences a decrease of only 7% when propagating over the bottom 115 m of the channel. For the flashes triggered on or after 13 August 2014, the same behavior is observed and the aforementioned percentages are 41%, 28%, and 24%, respectively. Averaged over all channel heights, higher-frequency luminosity components attenuate approximately 3 times faster than lower frequency components.

In summary, for 24 out of the 36 cases (three channel sections times 12 return strokes), the percentage difference of ΔR calculated at 200 kHz is less than that calculated at 100 kHz; for 24/36, the percentage difference of ΔR calculated at 300 kHz is less than that calculated at 200 kHz; for 26/36, the percentage difference of ΔR calculated at 300 kHz is less than that calculated at 100 kHz; and for 17/36, the percentage difference of ΔR calculated at 300 kHz is less than that calculated at 200 kHz and the ΔR calculated at 200 kHz is less than that calculated at 100 kHz. The results from the two sets of data are essentially the same since we average over all channel segments going from 4 m to 115 m, even if the heights studied are different for each data set.

In Table 3 we show the phase, group, and time domain velocities calculated for all 12 return strokes as a function of channel height. In addition, for each return stroke, we provide the narrowband phase and group velocities as a function of signal frequency component, found from the methodology described in section 2. In 10 out of the 12 return strokes analyzed, both phase and group velocities increase with increasing channel height, up to 115 m. For the fourth return stroke of UF 14-35, and the second return stroke of UF 14-52, the phase and group velocities decrease with increasing height. In columns 11 and 18 of Table 3, we provide the average lower and upper limits of the frequency narrowband phase and group velocities measured at each channel section. These limits were calculated the same way as those shown in Figure 3 and characterized by the red and yellow curves. For flashes triggered prior to 13 August

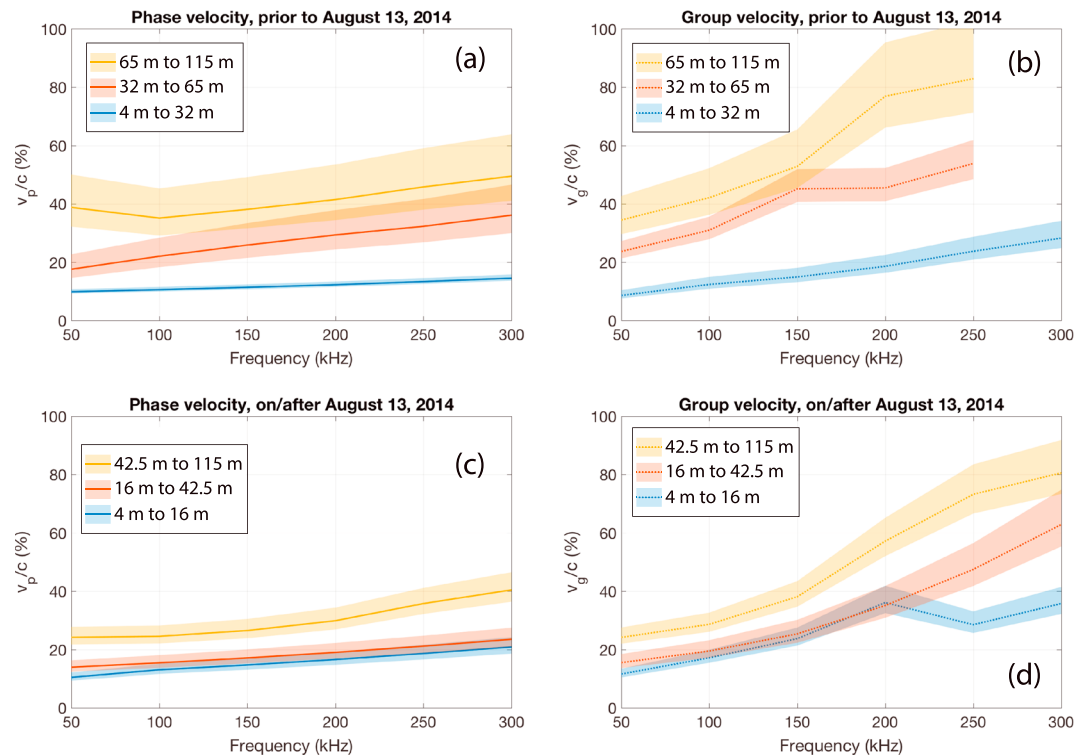


Figure 6. Phase (v_p) and group (v_g) velocities averaged over each of the three channel section and over each of the two data sets: one containing all six flashes triggered prior to 13 August 2014 and the other containing all six flashes triggered on or after that date. (a) Phase velocity (v_p) averaged over all six return strokes triggered prior to 13 August 2014 and over each of the three channel sections (bottom: 4 m to 32 m, middle: 32 m to 65 m, and top: 65 m to 115 m). (b) The group velocity (v_g) averaged over all six return strokes triggered prior to 13 August 2014 and over each of the three channel sections (bottom: 4 m to 32 m, middle: 32 m to 65 m, and top: 65 m to 115 m). (c) The phase velocity (v_p) averaged over all six return strokes triggered on or after 13 August 2014 and over each of the three channel sections (bottom: 4 m to 16 m, middle: 16 m to 42.5 m, and top: 42.5 m to 115 m). (d) The group velocity (v_g) averaged over all six return strokes triggered on or after 13 August 2014 and over each of the three channel sections (bottom: 4 m to 16 m, middle: 16 m to 42.5 m, and top: 42.5 m to 115 m). In each subplot, the shaded areas represent the upper and lower limits of the error analysis performed for each curve.

2014, the lower limit is, on average, 14% less than the measured value (or 86% of the measured value) and the upper limit is, on average, 22% greater than the measured value (or 122% of the measured value). For flashes triggered on or after that date, the percentage values are, on average, -11% (or 89% of the measured value) and +16% (116% of the measured value), respectively, indicating that in the worst case, our overall errors are constrained in the range from -14% to +22% of the measured value.

As previously stated, the high-frequency cutoff of our frequency domain analysis is limited by the SNR calculated as a function of frequency for the luminosity waveform with the slowest rising edge, usually the signal measured by the photodiode aimed at the highest channel height (D7 for events triggered prior to 13 August 2014 and D11 for events triggered after that date). This is the reason why, for some of the return strokes analyzed here, and shown in Table 3, the phase and group velocities cannot be appropriately calculated for narrowband signal frequencies greater than 150 kHz. Similar to Table 2, the statistics provided in Table 3 are calculated separately for the two individual data sets: one consisting of flashes triggered prior to 13 August 2014 and one consisting of flashes triggered on or after that date. The channel height intervals going from 4 m to 115 m were different for the two data sets. In general, both phase and group velocities measured in the three channel sections described in section 2 (bottom, middle, and top) increase with increasing frequency, group velocity generally being higher than phase velocity.

In summary, for the flashes triggered prior to 13 August 2014, the phase velocity calculated at 250 kHz, averaged over all channel sections, is roughly 2 times larger than the phase velocity calculated for the narrowband signal frequency of 50 kHz, whereas the group velocity at 250 kHz is 2.2 times larger than the

group velocity at 50 kHz. Similarly, for the flashes triggered on or after 13 August 2014, the phase velocity calculated at 300 kHz, averaged over all channel sections, is on average 1.7 times larger than the phase velocity calculated for the narrowband signal frequency of 50 kHz, whereas the group velocity at 300 kHz is, on average, 3.1 times larger than the group velocity at 50 kHz.

It is important to emphasize that the statistics given at the bottom of each section of Table 3 lump the results of all strokes calculated at all channel heights for selected narrowband signal frequencies. In order to analyze the average behavior as a function of both frequency and channel height, we construct Table 4 by averaging, within each of the two data sets, the phase velocities calculated for the six strokes comprising each data set at selected signal frequencies as a function of channel height. We do the same for the group velocity and plot the results shown in Table 4 in Figure 6.

Figure 6 illustrates many important characteristics that result from this luminosity frequency domain analysis. Following the same convention used to plot Figure 3, we plot in Figure 6 solid lines to represent phase velocity results and dotted lines to represent group velocity results. In the four subplots of Figure 6, each color represents one of the three channel sections described in section 2: bottom (plotted in blue), middle (plotted in red), and top (plotted in yellow). Figure 6a plots the phase velocity results of the first data set, i.e., events triggered prior to 13 August 2014, for which the three channel sections are 4 m to 32 m, 32 m to 65 m, and 65 m to 115 m. Figure 6b plots the group velocity results of the first data set, i.e., events triggered prior to 13 August 2014, for which the three channel sections are 4 m to 32 m, 32 m to 65 m, and 65 m to 115 m. In contrast, Figure 6c plots the phase velocity results of the second data set, i.e., events triggered on or after 13 August 2014, for which the three channel sections are 4 m to 16 m, 16 m to 42.5 m, and 42.5 m to 115 m. Lastly, Figure 6d plots the group velocity results of the second data set, i.e., events triggered on or after 13 August 2014, for which the three channel sections are 4 m to 16 m, 16 m to 42.5 m, and 42.5 m to 115 m. We note that the curves shown in Figures 6a–6d are a consequence of averaging the results for all six strokes of each data set depicted in Table 3 for each of the three channel sections, just as presented in Table 4. In each subplot of Figure 6, the shaded areas represent the upper and lower limits of the error analysis performed for each curve. These two limits are found in the bottom of each section of Table 3 (column 11 for phase velocity errors and column 18 for group velocity errors). For both data sets, the phase and group velocities generally increase with increasing frequency for all of the channel sections considered. Similarly, both phase and group velocities increase, on average, with increasing channel height, indicating that the luminosity waveform is observed to speed up in the bottom 115 m of the triggered lightning channel. Also from comparing Figures 6b to 6a, and Figures 6d to 6c, we see that the group velocity is, on average, higher than the phase velocity for a fixed signal frequency and channel height. For the first data set, shown in Figures 6a and 6b, the group velocity calculated at 250 kHz is, on average, 1.8, 1.7, and 1.8 times larger than the phase velocity calculated at 250 kHz and at the bottom (4 m to 32 m), middle (32 m to 65 m), and top (65 m to 115 m) channel sections, respectively. For the second data set, shown in Figures 6c and 6d, the group velocity calculated at 300 kHz is, on average, 1.7, 2.7, and 2.0 times larger than the phase velocity calculated at 300 kHz and at the bottom (4 m to 16 m), middle (16 m to 42.5 m), and top (42.5 m to 115 m) channel sections, respectively. On average, both phase and group velocities peak at the highest channel section and largest-frequency component.

5. Discussion

Carvalho et al. [2015] found, for the fourth return stroke of UF 14-51, an average return stroke luminosity velocity of $1.1 \times 10^8 \text{ m s}^{-1}$ between the photodiode aimed at the channel-bottom (photodiode D1) and the one aimed at the 115 m altitude (photodiode D11), a measurement made at the 20% level of the time domain waveforms. In order to compare our results to those of *Carvalho et al.* [2015] and to increase the size of their data set from 2 to 12, we analyze the velocities in the time domain between the pairs of photodiodes considered in section 3 using two approaches: (a) the 20% level time delay measurements and (b) the cross-correlation time delay. Cross correlation has not been used previously to determine return stroke velocity except for the statement in *Kawasaki et al.* [1987] that cross correlation in their two-height measurement gave a similar result (though twice as large) as their group velocity determination. The time domain upward luminosity velocity reported in *Carvalho et al.* [2015] had no information regarding the luminosity frequency content. The time delays between pairs of photodiodes for two return strokes (a subset of the present 12 return strokes considered in this paper), measured at the 20% amplitude level, are presented in column 15 of Table 3 of *Carvalho et al.* [2015].

In order to calculate the upward luminosity velocity from the time domain luminosity waveforms using the cross-correlation technique, we cross correlate in time the luminosity curves measured by pairs of photodiodes; the time shift (Δt_{lag}) between two curves is defined as the point in time where the cross-correlation amplitude reaches its maximum peak value, with the results being shown in our Table 3, column 21. A negative value for Δt_{lag} (as seen in column 21 of our Table 3) indicates that the second input to the cross-correlation operation must be shifted in time to the left in order to achieve maximum cross-correlation magnitude with the first input. Because the luminosity waveforms measured by pairs of photodiodes are not much dissimilar in shape and are separated by a relatively small time delay, the output of the cross-correlation function between each of the three pairs of photodiodes (i.e., bottom, middle, and top channel sections) is relatively sharp and well defined for ranges as narrow as a few tens of nanoseconds.

In column 20 of our Table 3 we present the velocity calculated from the 20% amplitude level time delay, and in column 22 we present the velocity results from the cross-correlation operation for different channel heights. For the fourth return stroke of UF 14-51, the mean of the upward velocity calculated from the time delay measured at the 20% amplitude-level between pairs of photodiodes is $1.0 \times 10^8 \text{ m s}^{-1}$ and the mean of the upward velocity calculated from the cross correlation is $0.7 \times 10^8 \text{ m s}^{-1}$, which agree well with the behavior of the average velocity up to 115 m reported by *Carvalho et al.* [2015]. Similar to the frequency domain velocities, the time domain velocities are also observed to increase with increasing height up to 115 m. We note that a decrease in the luminosity velocity at heights greater than 115 m is expected but could not be measured because our field of view ended at that height.

For the full data set of 12 return strokes, the velocity averaged over all channel heights is $1.4 \times 10^8 \text{ m s}^{-1}$ if computed at the 20% amplitude level and $0.8 \times 10^8 \text{ m s}^{-1}$ if computed by cross correlation.

Two out of the 36 time domain velocities calculated by using the 20% amplitude-level technique and presented in Table 3 are greater than the speed of light. These unrealistic velocities are likely a result of measurement error associated with the two time domain luminosity waveforms being particularly close in time to each other at the bottom of the channel. *Wang et al.* [2014] reported the attachment process of rocket-triggered lightning occurring in the channel heights ranging from 8 to approximately 23 m, as well as the evidence of a bidirectional propagation of the return stroke wave from its initiation height. This effect is almost certainly present in the 12 return strokes analyzed here, and may account for the unrealistic time domain velocities observed at the bottom of the channel (from 4 to 16 m) during the fourth return stroke of UF 14-35 and the second return stroke of UF 14-52, and may also produce errors in the measurements in the bottom channel section.

The majority (10 out of 12 return strokes) of the velocities calculated at the bottom-most section of the channel (either from 4 to 32 m for events prior to 13 August 2014 or from 4 to 16 m for event triggered on or after that date) are lower than the velocities calculated for the middle and top channel sections; i.e., the return stroke luminosity is observed to speed up above the bottom of the channel. We caution the reader that the velocities computed at the channel-bottom may be affected by the unresolved bidirectional propagation of the return stroke wave. Our experimental setup was not designed to decompose these two waves propagating bidirectionally from their initiation height, but such decomposition has been done for both natural and triggered lightning [e.g., *Wang et al.*, 2014, 2015]. We note that both cases with the time domain velocities greater than the speed of light were observed for the events triggered on or after 13 August 2014, when the photodiodes aimed at the channel-bottom were separated by only 12 m, less than the lowest channel section separation of 28 m before 13 August 2014. For the events triggered prior to 13 August 2014, all velocities calculated at the channel bottom are below the speed of light.

Kawasaki et al. [1987] were apparently the first to publish an analysis of the upward luminosity return stroke velocity as a function of signal frequency. Equation (5) of *Kawasaki et al.* [1987] describing the group velocity is a version of *Stratton's* [1941] equation 41 in his Chapter 5. Equation (5) of *Kawasaki et al.* [1987] separates the changes in phase due to (1) the different starting times of their luminous signals and (2) the fact that the dispersion causes the lower frequencies to arrive later than the higher frequencies. The frequencies they studied ranged from 1 kHz to 200 kHz. Consequently, the approach taken by *Kawasaki et al.* [1987] was similar to ours, except that they calculated a single average group velocity, defined as the slope of an $\omega - k$ diagram for all their data, or mathematically as the derivative of the angular frequency, ω , with respect to the wave number, k , defined as $2\pi/\lambda$, and not group velocity versus height as we do.

Kawasaki *et al.* [1987] reported that their average group velocity was half of their time domain tip velocity, but we note that directly comparing these two velocities can be confusing, since one is defined in the frequency domain and the other in the time domain (group and tip velocities, respectively). A more robust approach consists of comparing the group velocity to the phase velocity, since both are well defined in the frequency domain. As seen in Figure 5, our group velocity results, for the fourth return stroke of UF 14-51, are up to approximately 2 times greater than the phase velocity calculated at the same frequency. In addition, the v_g/v_p ratio found in this paper decreases with decreasing values of f for constant channel sections, indicating that at lower frequencies, the group velocity may approach the phase velocity value. The data for the remaining 11 of 12 strokes are found in Table 3 and Figure 6

The maximum experimental error of the frequency domain method is associated with errors in the height at which each photodiode is aimed (called center height difference or Δz) and is likely to minimally affect our results because for all pairs of photodiodes analyzed here, the best fit curve fits the measured transfer function data very well: values of R^2 averaging 0.87 with 0.11 standard deviation and mean square error values averaging 9×10^{-3} with 9×10^{-3} standard deviation.

The 300 kHz high-frequency cutoff that confined the presented frequency domain analysis in the example of the fourth return stroke of UF 14-51 is limited by the signal with the slowest rising edge (photodiode D11, 115 m). For signals having faster risetimes, the bandwidth in which our results would be valid would increase; conversely, signals with a slower risetimes than that of D11 would have a smaller bandwidth for which results would be valid (as seen in Table 3 for all our data).

6. Summary

In this paper, our goal was to find the attenuation and the velocity associated with individual frequency components of the return stroke luminosity signal measured at different channel altitudes. We derived upward luminosity velocities for 12 return strokes by using Fourier analysis, and the results from this frequency domain method show that (1) the return stroke velocity of the return stroke luminosity generally increases with increasing height up to 115 m, (2) higher-frequency luminosity components (as large as 300 kHz, for some return strokes) exhibited a faster phase velocity (1.8 times faster, on average) than lower frequency components (e.g., 50 kHz), (3) higher-frequency luminosity components (as large as 300 kHz, for some return strokes) propagated with a faster group velocity (2.3 times faster, on average) than lower frequency components (e.g., 50 kHz); (4) averaged over all channel heights, the group velocity of higher-frequency components exceeds the phase velocity by a factor of roughly 2, (5) averaged over all channel heights, the group velocity approaches the phase velocity at lower frequencies, and (6) on average, higher-frequency luminosity components attenuate approximately 3 times faster than lower frequency components.

Acknowledgments

This work was supported by DARPA and the U.S. Air Force through contract FA8650-15-C-7535, by DARPA NIMBUS grant HR0011-1-10-1-0061, and by Tau Beta Pi through the 2016-2017 fellowship No. 37 (Williams). The data for this paper are summarized in Tables 2 and 3; any additional data may be obtained from F.L. Carvalho (e-mail: fcarval1@ufl.edu). Because creating triggered lightning is a team effort, the authors wish to thank all involved, in alphabetical order: J.A. Caicedo, W.R. Gamerota, B.M. Hare, D.A. Kotovsky, T.K. Ngjin, J.T. Pilkey, and R.A. Wilkes.

References

- Bergland, G. D. (1969), A guided tour of the fast Fourier transform, *IEEE Spectrum*, 6, 41–52, doi:10.1109/MSPEC.1969.5213896.
- Boyle, J. S., and R. E. Orville (1976), Return stroke velocity measurements in multistroke lightning flashes, *J. Geophys. Res.*, 81, 4461–4466, doi:10.1029/JC081i024p04461.
- Carvalho, F. L., D. M. Jordan, M. A. Uman, T. Ngjin, W. R. Gamerota, and J. T. Pilkey (2014), Simultaneously measured lightning return stroke channel-base current and luminosity, *Geophys. Res. Lett.*, 41, 7799–7805, doi:10.1002/2014GL062190.
- Carvalho, F. L., M. A. Uman, D. M. Jordan, and T. Ngjin (2015), Lightning current and luminosity at and above channel bottom for return strokes and M-components, *J. Geophys. Res. Atmos.*, 120, 10,645–10,663, doi:10.1002/2015JD023814.
- Chen, J., and M. Zhu (2014), Calculation of lightning flashover rates of overhead distribution lines considering direct and indirect strokes, *IEEE Trans. Electromagn. Compat.*, 56(3), doi:10.1109/TEMC.2014.2309146.
- Hubert, P., and G. Mouget (1981), Return stroke velocity measurements in two triggered lightning flashes, *J. Geophys. Res.*, 86, 5253–5261, doi:10.1029/JC086iC06p05253.
- Idone, V. P., and R. E. Orville (1982), Lightning return stroke velocities in the thunderstorm research international program (TRIP), *J. Geophys. Res.*, 87, 4903–4915, doi:10.1029/JC087iC07p04903.
- Idone, V. P., R. E. Orville, P. Hubert, L. Barret, and A. Eybert-Berard (1984), Correlated observations of three triggered lightning flashes, *J. Geophys. Res.*, 89, 1385–1394, doi:10.1029/JD089iD01p01385.
- Kawasaki, Z.-I., M. Nakano, and T. Takeuti (1987), Group velocity of subsequent return strokes in triggered lightning, *Trans. I.E.E. Japan*, 107(4), 47–53.
- Krider, E. P. (1992), On the electromagnetic fields, Poynting vector, and peak power radiated by lightning return strokes, *J. Geophys. Res.*, 97, 15,913–15,917, doi:10.1029/92JD01490.
- Krider, E. P. (1994), On the peak electromagnetic fields radiated by lightning return strokes toward the middle-atmosphere, *J. Atmos. Electr.*, 14, 17–24.

- Liang, C., B. Carlson, N. Lehtinen, M. Cohen, R. A. Marshall, and U. Inan (2014), Differing current and optical return stroke speeds in lightning, *Geophys. Res. Lett.*, *41*, 2561–2567, doi:10.1002/2014GL059703.
- Mach, D. M., and W. D. Rust (1989), A photoelectric technique for measuring lightning-channel propagation velocities from a mobile laboratory, *J. Atmos. Oceanic Technol.*, *6*(3), 439–445.
- Olsen, R. C. I. I., D. M. Jordan, V. A. Rakov, M. A. Uman, and N. Grimes (2004), Observed one-dimensional return stroke propagation speeds in the bottom 170 m of a rocket-triggered lightning channel, *Geophys. Res. Lett.*, *31*, L16107, doi:10.1029/2004GL020187.
- Papoulis, A. (1977), *Signal Analysis*, McGraw-Hill, New York.
- Schonland, B. F. J. (1956), *The Lightning Discharge, Handbuch der Physik*, vol. 22, pp. 576–628, Springer, Berlin.
- Stratton, J. A. (1941), *Electromagnetic Theory*, McGraw-Hill, New York.
- Thottappillil, R., and M. A. Uman (1993), Comparison of lightning return-stroke models, *J. Geophys. Res.*, *98*(D12), 22,903–22,914, doi:10.1029/93JD02185.
- Wang, D., V. A. Rakov, M. A. Uman, N. Takagi, T. Watanabe, D. E. Crawford, K. J. Rambo, G. H. Schnetzer, R. J. Fisher, and Z.-I. Kawasaki (1999), Attachment process in rocket-triggered lightning strokes, *J. Geophys. Res.*, *104*(D2), 2143–2150, doi:10.1029/1998JD200070.
- Wang, D., N. Takagi, X. Liu, T. Watanabe, and A. Chihara (2004), Luminosity characteristics of multiple dart leader/return stroke sequences measured with a high-speed digital image system, *Geophys. Res. Lett.*, *31*, L02111, doi:10.1029/2003GL018613.
- Wang, D., N. Takagi, W. R. Gamerota, M. A. Uman, J. D. Hill, and D. M. Jordan (2013), Initiation processes of return strokes in rocket-triggered lightning, *J. Geophys. Res. Atmos.*, *118*, 9880–9888, doi:10.1002/jgrd.50766.
- Wang, D., W. R. Gamerota, M. A. Uman, N. Takagi, J. D. Hill, J. Pilkey, T. Ngin, D. M. Jordan, S. Mallick, and V. A. Rakov (2014), Lightning attachment processes of an “anomalous” triggered lightning discharge, *J. Geophys. Res. Atmos.*, *119*, 1524–1533, doi:10.1002/2013JD020787.
- Wang, D., N. Takagi, W. R. Gamerota, M. A. Uman, and D. M. Jordan (2015), Lightning attachment processes of three natural lightning discharges, *J. Geophys. Res. Atmos.*, *120*, 10,637–10,644, doi:10.1002/2015JD023734.
- Willett, J. C., V. P. Idone, R. E. Orville, C. Leteinturier, A. Eybert-Berard, L. Barret, and E. P. Krider (1988), An experimental test of the “transmission-line model” of electromagnetic radiation from triggered lightning return strokes, *J. Geophys. Res.*, *93*, 3867–3878, doi:10.1029/JD093iD04p03867.